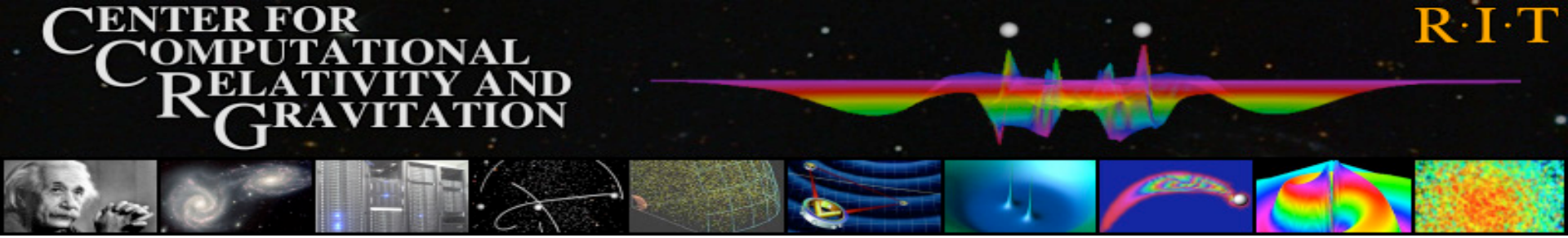

Remnant of binary black-hole mergers: The spinless case revisited

Carlos Lousto

Rochester Institute of Technology

Capra 20, Chapel Hill, NC, June 19th 2017

Overview:
S-Matrix description of BBH merger

$m_1, m_2,$
$\mathbf{S}_1, \mathbf{S}_2$ ➔

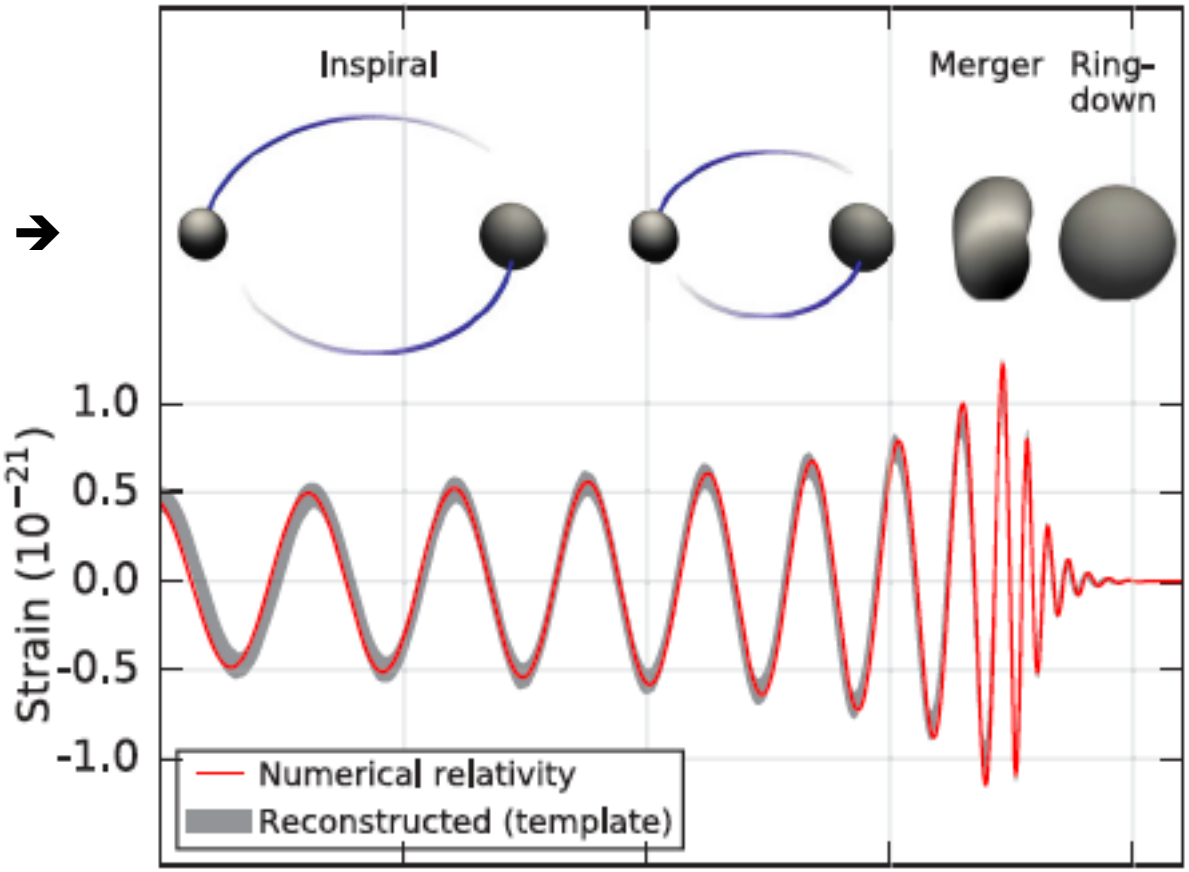

➔ $M_f\,(q,\mathbf{S}_1,\mathbf{S}_2)$
➔ $\mathbf{S}_f\,(q,\mathbf{S}_1,\mathbf{S}_2)$
$\mathbf{V}_f\,(q,\mathbf{S}_1,\mathbf{S}_2)$

➔ **L**peak
➔ **ω**peak

We developed phenomenological expansions based on a (4^{th} order) Taylor expansion in terms of variables q, $\mathbf{S}_1$, $\mathbf{S}_2$ but restricted to Parity and exchange 1↔2 symmetries.

L. Boyle and M. Kesden, Phys. Rev. **D78**, 024017 (2008)

Simulations

- 61 New aligned spin simulations + 10 new nonspinning
- $1/3 \leq q \leq 1$ and $-0.85 \leq a_i \leq +0.85$ for the spinning cases
- $1/6 \leq q < 1$ for the nonspinning
- Runs give 8-10 orbits prior to merger at $e \approx 10^{-3}$

- This is in addition to the 36 runs we did in 2014

- Those two sets of runs will form the core of the new RIT waveform catalog soon to be public.

- Key: Black (2014), Blue (2016)
  Grey (by symmetry).

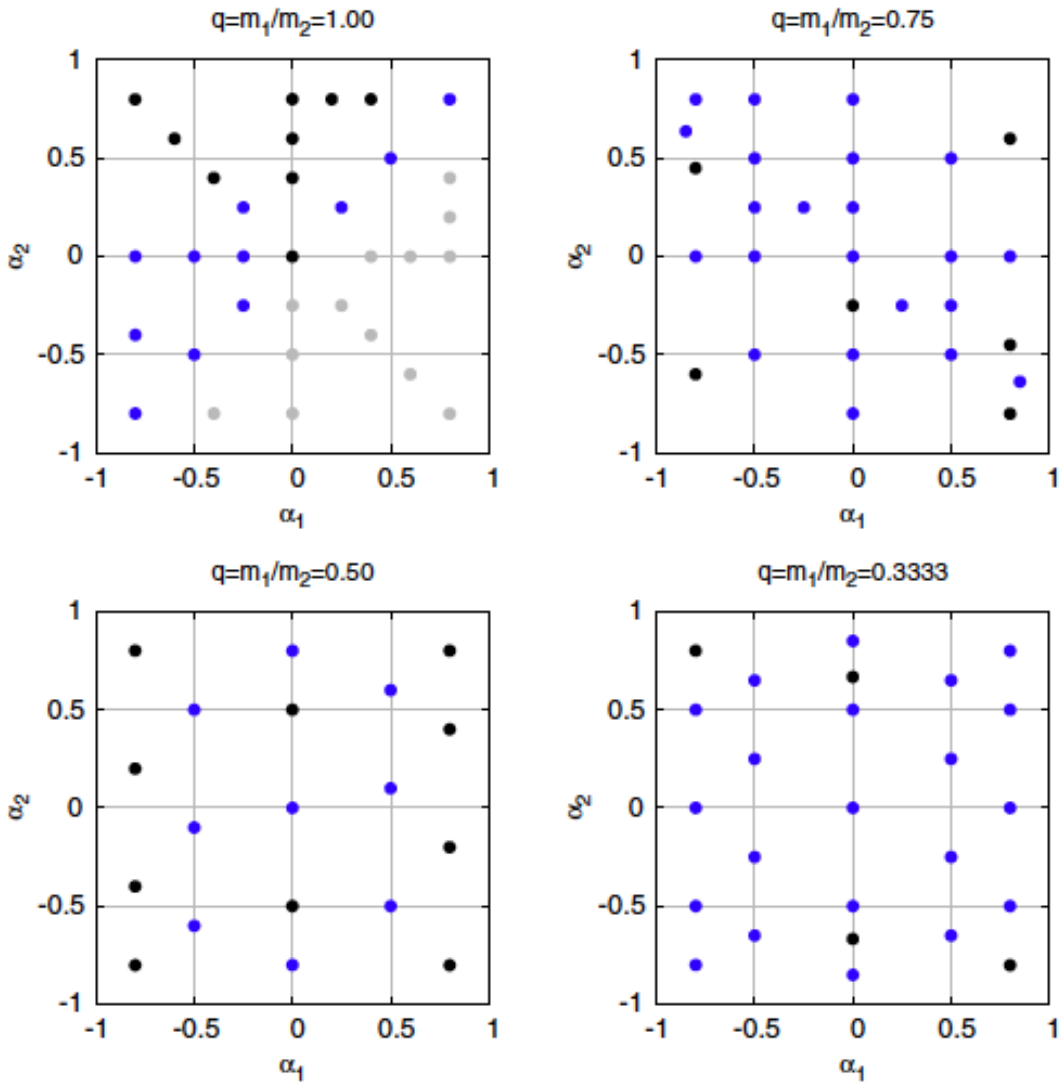

J. Healy, C. O. Lousto, and Y. Zlochower, Phys. Rev. **D90**, 104004 (2014), arXiv:1406.7295 [gr-qc].

J. Healy and C. O. Lousto, Phys. Rev. **D95**, 024037 (2017), arXiv:1610.09713 [gr-qc].

CATALOGS OF NUMERICAL RELATIVITY WAVEFORMS

Center for Computational Relativity and Gravitation R·I·T

Simulating eXtreme Spacetimes

Cardiff University / Prifysgol Caerdydd

[RIT Catalog of NR waveforms by Healy et al. arXiv:1703.03423 ,
Adding to the SXS and GaTech catalogs]

Georgia Tech Center for Relativistic Astrophysics College of Sciences

UIB Universitat de les Illes Balears

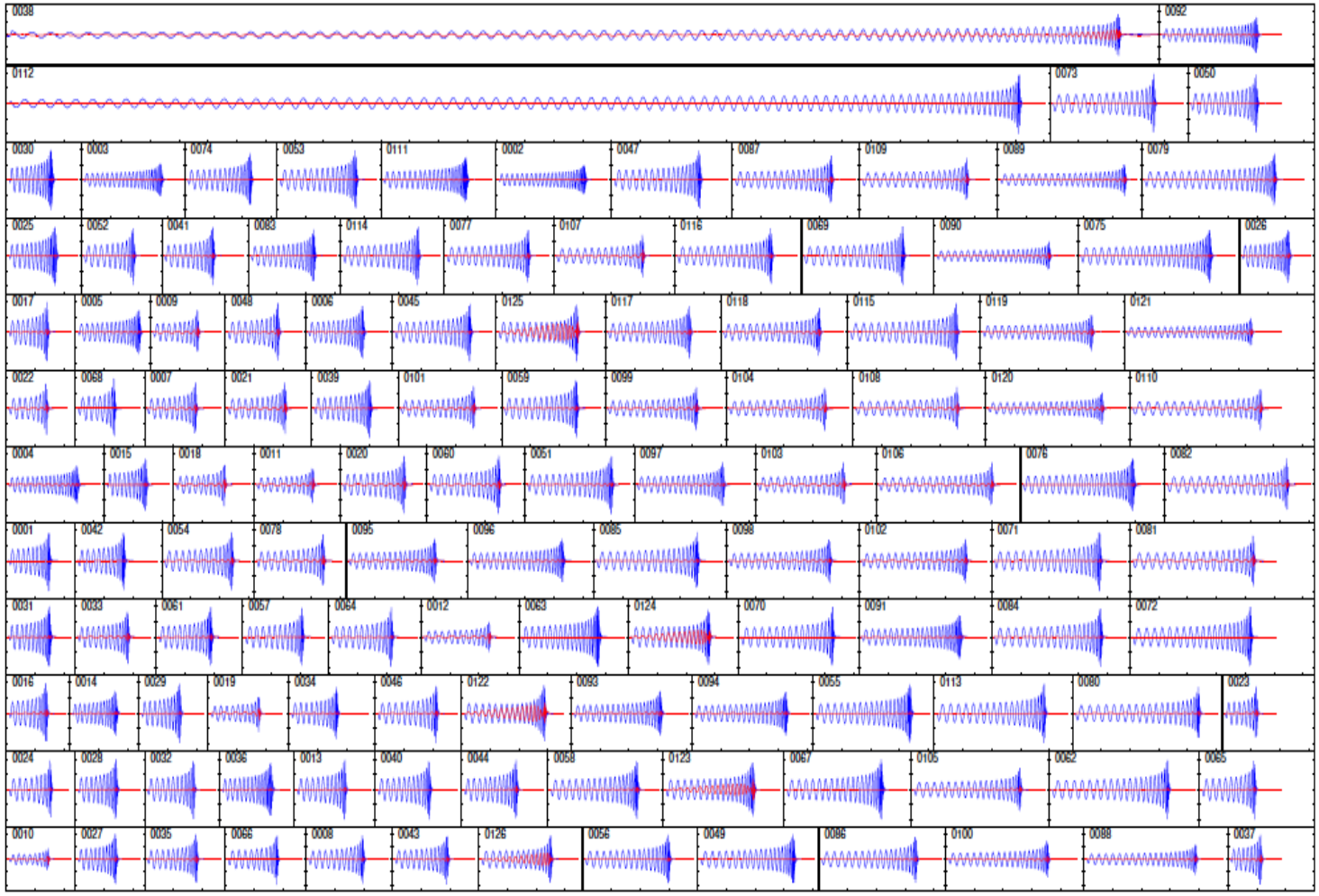

NR/LSC teams assembled more than a thousand NR waveforms, now fully integrated in LIGO Algorithm Library (LAL)

This can be used to directly estimate parameters of BBHs from NR without the use of models: Abbot et al. **arXiv:1606.01262**

Final remnant mass and spin modeling

The fitting formula for $M_{\rm rem}$ is given by

$$\begin{aligned}\frac{M_{\rm rem}}{m} = (4\eta)^2\{&M_0 + K_1\tilde{S}_{\parallel} + K_{2a}\tilde{\Delta}_{\parallel}\delta m + K_{2b}\tilde{S}_{\parallel}^2 \\ &+ K_{2c}\tilde{\Delta}_{\parallel}^2 + K_{2d}\delta m^2 + K_{3a}\tilde{\Delta}_{\parallel}\tilde{S}_{\parallel}\delta m + K_{3b}\tilde{S}_{\parallel}\tilde{\Delta}_{\parallel}^2 \\ &+ K_{3c}\tilde{S}_{\parallel}^3 + K_{3d}\tilde{S}_{\parallel}\delta m^2 + K_{4a}\tilde{\Delta}_{\parallel}\tilde{S}_{\parallel}^2\delta m + K_{4b}\tilde{\Delta}_{\parallel}^3\delta m \\ &+ K_{4c}\tilde{\Delta}_{\parallel}^4 + K_{4d}\tilde{S}_{\parallel}^4 + K_{4e}\tilde{\Delta}_{\parallel}^2\tilde{S}_{\parallel}^2 + K_{4f}\delta m^4 \\ &+ K_{4g}\tilde{\Delta}_{\parallel}\delta m^3 + K_{4h}\tilde{\Delta}_{\parallel}^2\delta m^2 + K_{4i}\tilde{S}_{\parallel}^2\delta m^2\} \\ &+ [1 + \eta(\tilde{E}_{\rm ISCO} + 11)]\delta m^6, \end{aligned} \quad (1)$$

where

$$\begin{aligned} m &= m_1 + m_2, \\ \delta m &= \frac{m_1 - m_2}{m}, \\ \tilde{S} &= (\vec{S}_1 + \vec{S}_2)/m^2, \\ \tilde{\Delta} &= (\vec{S}_2/m_2 - \vec{S}_1/m_1)/m, \end{aligned}$$

where m_i is the mass of BH $i = 1, 2$ and $\vec{S}_i$ is the spin of BH i. We also use the auxiliary variables

and

$$\begin{aligned} \eta &= \frac{m_1 m_2}{m^2}, \\ q &= \frac{m_1}{m_2}, \\ \vec{\alpha}_i &= \vec{S}_i/m_i^2, \end{aligned}$$

where $|\vec{\alpha}_i| \leq 1$ is the dimensionless spin of BH i, and we use the convention that $m_1 \leq m_2$ and hence $q \leq 1$. Here the index $\perp$ and $\parallel$ refer to components perpendicular to and parallel to the orbital angular momentum.

Final remnant mass and spin modeling

$$\alpha_{\rm rem} = \frac{S_{\rm rem}}{M_{\rm rem}^2} = (4\eta)^2\{L_0 + L_1\tilde{S}_{\|} + L_{2a}\tilde{\Delta}_{\|}\delta m + L_{2b}\tilde{S}_{\|}^2 + L_{2c}\tilde{\Delta}_{\|}^2 + L_{2d}\delta m^2 + L_{3a}\tilde{\Delta}_{\|}\tilde{S}_{\|}\delta m + L_{3b}\tilde{S}_{\|}\tilde{\Delta}_{\|}^2 + L_{3c}\tilde{S}_{\|}^3 + L_{3d}\tilde{S}_{\|}\delta m^2 + L_{4a}\tilde{\Delta}_{\|}\tilde{S}_{\|}^2\delta m + L_{4b}\tilde{\Delta}_{\|}^3\delta m + L_{4c}\tilde{\Delta}_{\|}^4 + L_{4d}\tilde{S}_{\|}^4 + L_{4e}\tilde{\Delta}_{\|}^2\tilde{S}_{\|}^2 + L_{4f}\delta m^4 + L_{4g}\tilde{\Delta}_{\|}\delta m^3 + L_{4h}\tilde{\Delta}_{\|}^2\delta m^2 + L_{4i}\tilde{S}_{\|}^2\delta m^2\} + \tilde{S}_{\|}(1+8\eta)\delta m^4 + \eta\tilde{J}_{\rm ISCO}\delta m^6. \quad (2)$$

Note that the two formulas, for the the final mass and final spin impose the *particle limit* through their ISCO contributions.

The use of *final horizon* measures for the final mass and spins greatly increases the accuracy (by 1-2 orders of magnitude) wrt radiation measures and is completely consistent with them.

Fitting to simulations

We fit 19+19 coefficients above to 175 of ours and SXS simulations and compare the new (V2) to the old (V1) fits

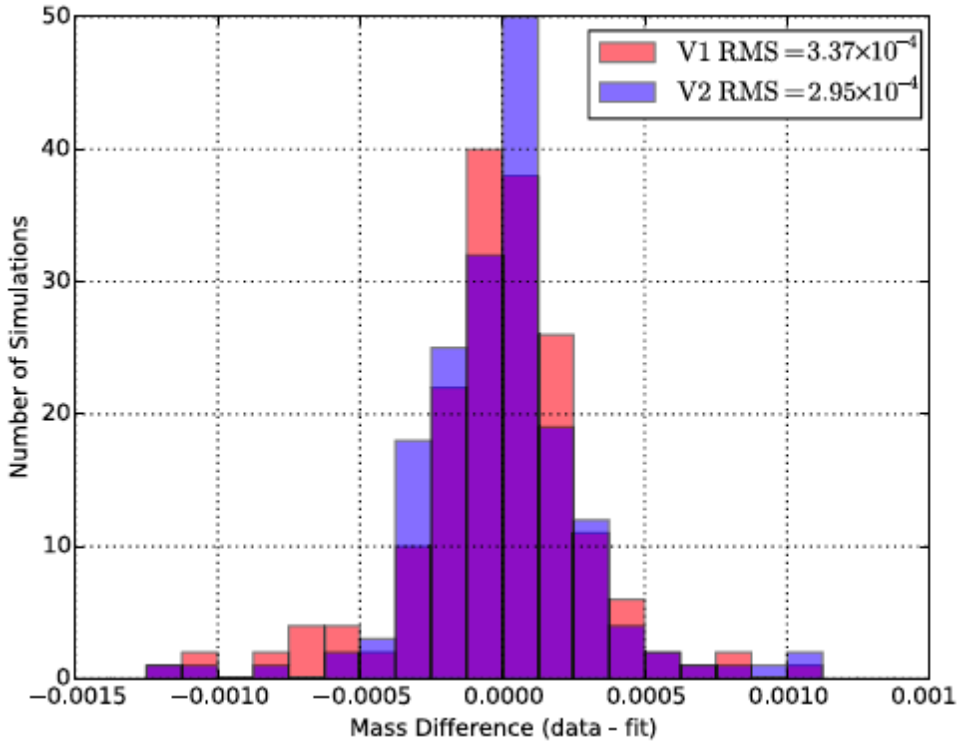

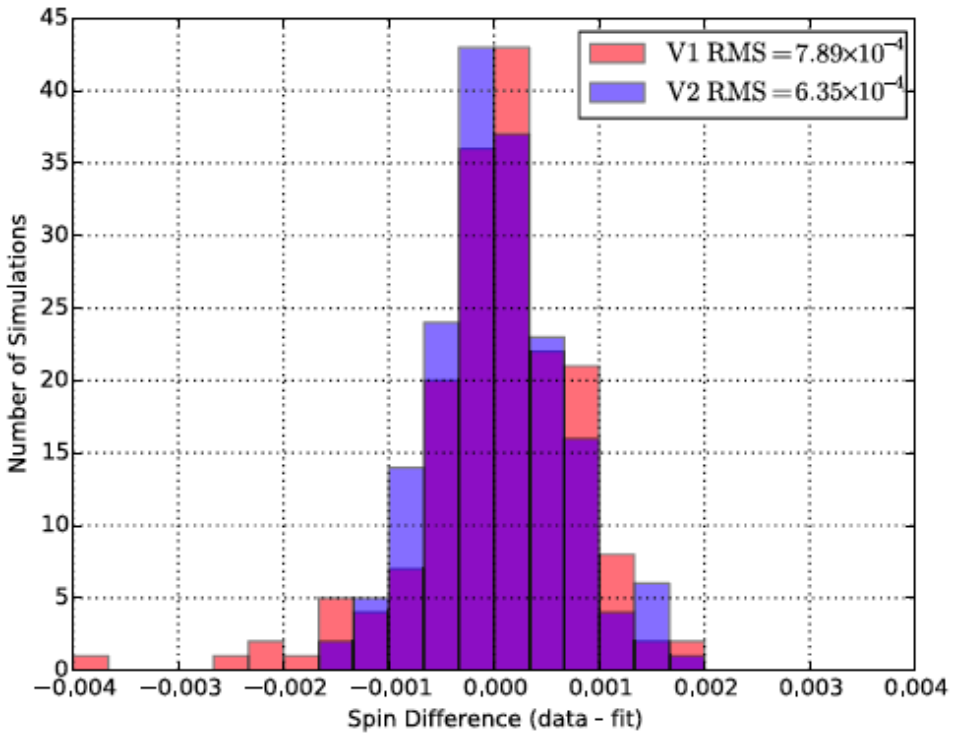

Final mass and spin modeling for nonprecessing binaries are already very good!

Recoil velocity and peak luminosity

We model the total recoil as

$$\vec{V}_{\rm recoil}(q,\vec{\alpha}_i) = v_m \hat{e}_1 + v_\perp(\cos(\xi)\hat{e}_1 + \sin(\xi)\hat{e}_2), \quad (4)$$

$\hat{e}_1, \hat{e}_2$ are orthogonal unit vectors in the orbital plane, and ξ measures the angle between the "unequal mass" and "spin" contributions to the recoil velocity in the orbital plane, and with

$$\begin{aligned} v_\perp = H\eta^2(&\tilde{\Delta}_\parallel + H_{2a}\tilde{S}_\parallel\delta m + H_{2b}\tilde{\Delta}_\parallel\tilde{S}_\parallel + H_{3a}\tilde{\Delta}_\parallel^2\delta m \\ &+H_{3b}\tilde{S}_\parallel^2\delta m + H_{3c}\tilde{\Delta}_\parallel\tilde{S}_\parallel^2 + H_{3d}\tilde{\Delta}_\parallel^3 + H_{3e}\tilde{\Delta}_\parallel\delta m^2 \\ &+ H_{4a}\tilde{S}_\parallel\tilde{\Delta}_\parallel^2\delta m + H_{4b}\tilde{S}_\parallel^3\delta m + H_{4c}\tilde{S}_\parallel\delta m^3 \\ &+H_{4d}\tilde{\Delta}_\parallel\tilde{S}_\parallel\delta m^2 + H_{4e}\tilde{\Delta}_\parallel\tilde{S}_\parallel^3 + H_{4f}\tilde{S}_\parallel\tilde{\Delta}_\parallel^3), \\ \xi = a + b\tilde{S}_\parallel &+ c\delta m\tilde{\Delta}_\parallel, \end{aligned} \quad (5)$$

where

$$v_m = \eta^2\delta m(A + B\delta m^2), \quad (6)$$

Peak luminosity modeling

We propose

$$
\begin{aligned}
L_{\rm peak} = (4\eta)^2\{&N_0 + N_1\tilde{S}_{\parallel} + N_{2a}\tilde{\Delta}_{\parallel}\delta m + N_{2b}\tilde{S}_{\parallel}^2 \\
&+ N_{2c}\tilde{\Delta}_{\parallel}^2 + N_{2d}\delta m^2 + N_{3a}\tilde{\Delta}_{\parallel}\tilde{S}_{\parallel}\delta m + N_{3b}\tilde{S}_{\parallel}\tilde{\Delta}_{\parallel}^2 \\
&+ N_{3c}\tilde{S}_{\parallel}^3 + N_{3d}\tilde{S}_{\parallel}\delta m^2 + N_{4a}\tilde{\Delta}_{\parallel}\tilde{S}_{\parallel}^2\delta m + N_{4b}\tilde{\Delta}_{\parallel}^3\delta m \\
&+ N_{4c}\tilde{\Delta}_{\parallel}^4 + N_{4d}\tilde{S}_{\parallel}^4 + N_{4e}\tilde{\Delta}_{\parallel}^2\tilde{S}_{\parallel}^2 + N_{4f}\delta m^4 \\
&+ N_{4g}\tilde{\Delta}_{\parallel}\delta m^3 + N_{4h}\tilde{\Delta}_{\parallel}^2\delta m^2 + N_{4i}\tilde{S}_{\parallel}^2\delta m^2\}. \qquad (3)
\end{aligned}
$$

Similar expansions can be carried out for the peak strain h, News, Ψ_4, and their corresponding peak frequencies ω_{peak} .

Fitting to simulations

We fit 17+19 coefficients above to ours 107 simulations
and compare the new (V2) to the old (V1) fits

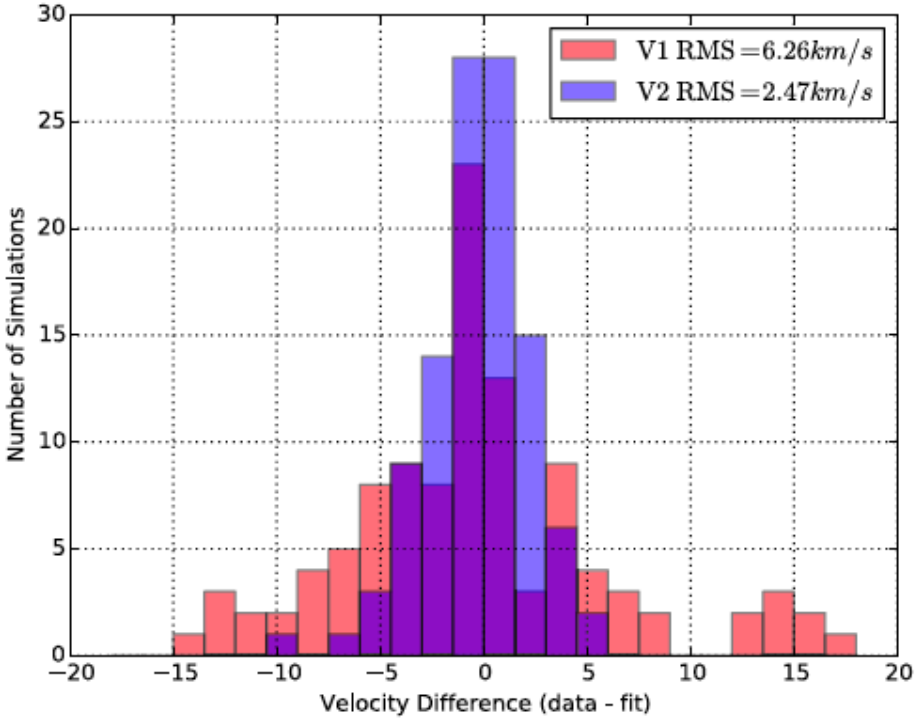

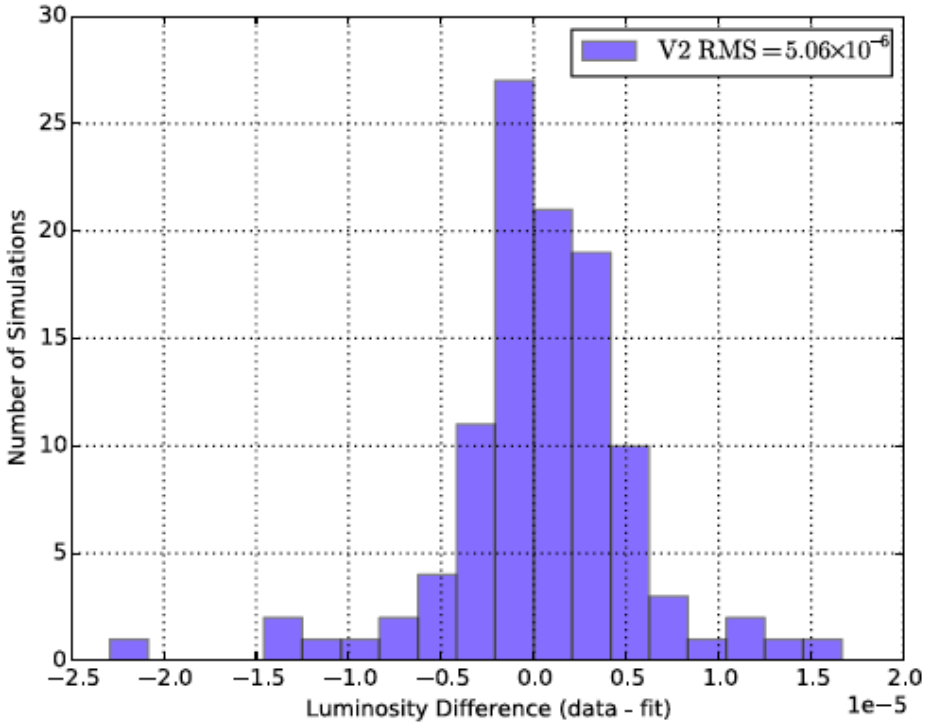

These represents corrections of a few percent since they are measured directly from radiation waveforms.
If one wants to improve upon this accuracy, one needs higher resolution simulations.

First discussion

- We have fitting formulae to predict the final properties of the merger of two black holes
  the errors in the final mass and spin are ≈ 0.1 – 0.2 %
  the errors in the recoil velocity and peak luminosity are ≈ 5%

- The fittings produce a maximum radiated energy of above 11.3%
  Mrem(1,1,1)=0.8867, while M(1,-1,-1)=0.968

- For equal mass binaries $\alpha f(1,1,1)=0.951$, $\alpha f(1,-1,-1)=0.358$

- The maximum recoil occurs for $q\approx 2/3$ at Vmax(2/3,+1,-1)=516 km/s

- Those studies made use of models up to $l\leq 6$,
  extrapolation to infinite observer,
  and weighted the fitting from the case studies of three finite difference resolutions.

- These well calibrated aligned spin formula are used for the nonprecessing extension.

- One can also look at hints of resummation by Padé approximants
  (In fact already alternatively used for modeling recoils and final masses).

The nonspinning BBH simulations revisited

- 14 nonspinning BBH simulations
- $1/100 \leq q=m_1/m_2 \leq 1$

3 resolutions for Richardson extrapolation

N100, N120, N140 for $q \leq 1/6$

N100, N144, and N173 for q = 1= 10,

N144, N173, and N207 for q = 1= 15,

N100, N144, and N207 for q = 1= 100.

- Perturbative extrapolation to infinite observer location
- Added up to l≤6 modes

To improve on these 3 main sources of error

TABLE II. Recoil velocity and peak luminosity for nonspinning binaries. Values are extrapolated to infinite resolution and infinite observer location and the error reflects the error in both operations added in quadrature.

q	V_{rem}	L_{peak}
0.0100	0.87 ± 0.04	$1.214 \times 10^{-6} \pm 5.641 \times 10^{-9}$
0.0667	33.47 ± 0.50	$4.417 \times 10^{-5} \pm 4.655 \times 10^{-7}$
0.1000	62.59 ± 0.56	$9.009 \times 10^{-5} \pm 9.736 \times 10^{-7}$
0.1667	119.06 ± 2.85	$2.185 \times 10^{-4} \pm 8.209 \times 10^{-6}$
0.2000	139.94 ± 3.90	$2.729 \times 10^{-4} \pm 3.193 \times 10^{-6}$
0.2500	161.77 ± 3.82	$3.718 \times 10^{-4} \pm 4.820 \times 10^{-6}$
0.3333	176.94 ± 3.91	$5.298 \times 10^{-4} \pm 5.389 \times 10^{-6}$
0.4000	174.20 ± 3.52	$6.358 \times 10^{-4} \pm 5.939 \times 10^{-6}$
0.5000	154.40 ± 2.94	$7.775 \times 10^{-4} \pm 6.944 \times 10^{-6}$
0.6000	125.28 ± 2.28	$8.809 \times 10^{-4} \pm 8.674 \times 10^{-6}$
0.6668	103.61 ± 1.55	$9.296 \times 10^{-4} \pm 9.733 \times 10^{-6}$
0.7500	76.13 ± 1.56	$9.749 \times 10^{-4} \pm 8.184 \times 10^{-6}$
0.8500	43.45 ± 0.59	$1.010 \times 10^{-3} \pm 1.074 \times 10^{-5}$
1.0000	0.00 ± 0.00	$1.027 \times 10^{-3} \pm 7.111 \times 10^{-6}$

J.Healy, C.O.Lousto, Y.Zlochower, arXiv:1705.07034

Expansions and particle limit in some detail

$M_{final}/M=M_0+M_2\,\delta m^2+M_4\,\delta m^4+O(\delta m^6)$, with M_0, M_2, M_4, fitting parameters

But we know that in the particle limit

- $m_{final}=m_{initial}=M$
- $\eta\,(E_{ISCO}/M-1)$ is the energy radiated from ∞

- Comparable mass radiative terms $E_{rad}\sim\eta^2$

In the particle limit $M_{final}/M=1$ and $\delta m^2 \rightarrow 1$ and by adding a δm^6-term we can impose this condition

$M_{final}/M=M_0+M_2\,\delta m^2+M_4\,\delta m^4+M_6\,\delta m^6$ to determine $M_6=1-M_0-M_2-M_4$

what allow to rewrite

$M_{final}/M=(1-\delta m^2)(M_0+M_2\,\delta m^2+M_4\,\delta m^4)+\delta m^6$ with $(1-\delta m^2)=4\eta$

Applying the same technique, now for the linear term in η we can impose $\eta\,(E_{ISCO}/m-1)$

And obtain $M_{final}/M=(4\eta)^2(M_0+M_2\,\delta m^2+M_4\,\delta m^4)+[1+\eta\,(E_{ISCO}/m+11)]\,\delta m^6$

A similar reasoning for the final spin leads to

$S_{final}/M_{final}^2=(4\eta)^2(L_0+L_2\,\delta m^2+L_4\,\delta m^4+[\eta\,J_{ISCO}/m^2]\,\delta m^6)$,

With L_0, L_2, L_4, fitting parameters.

L_{peak}, ω_{peak}, h_{peak}, etc all follow analogous expansions to M_{final} .

The Non-spinning case Revisted

A. Recoil velocities of non-spinning binaries

Consistent with our notation in Ref. [14], we expand the non-spinning recoil as

$$v_m = \eta^2 \delta m \left(A + B\,\delta m^2 + C\,\delta m^4\right). \qquad (1)$$

where $\delta m = (m_1 - m_2)/m$ and $m = (m_1 + m_2)$ and $4\eta = 1 - \delta m^2$.

TABLE V. Fitting to the recoil velocity of the remnant of nonspinning black hole binaries by Eq. (1). Fit 2 only uses A, B while Fit 3 also fits C. Standard error for each fit is also given.

Parameter	Fit [42]	Fit 2	Fit 3
A	-9210	-8919 ± 73	-8712 ± 32
B	-2790	-4273 ± 261	-6516 ± 256
C	0.0	0.0	3907 ± 424

[42] J. A. González, M. D. Hannam, U. Sperhake, B. Brugmann, and S. Husa, Phys. Rev. Lett. **98**, 231101 (2007),

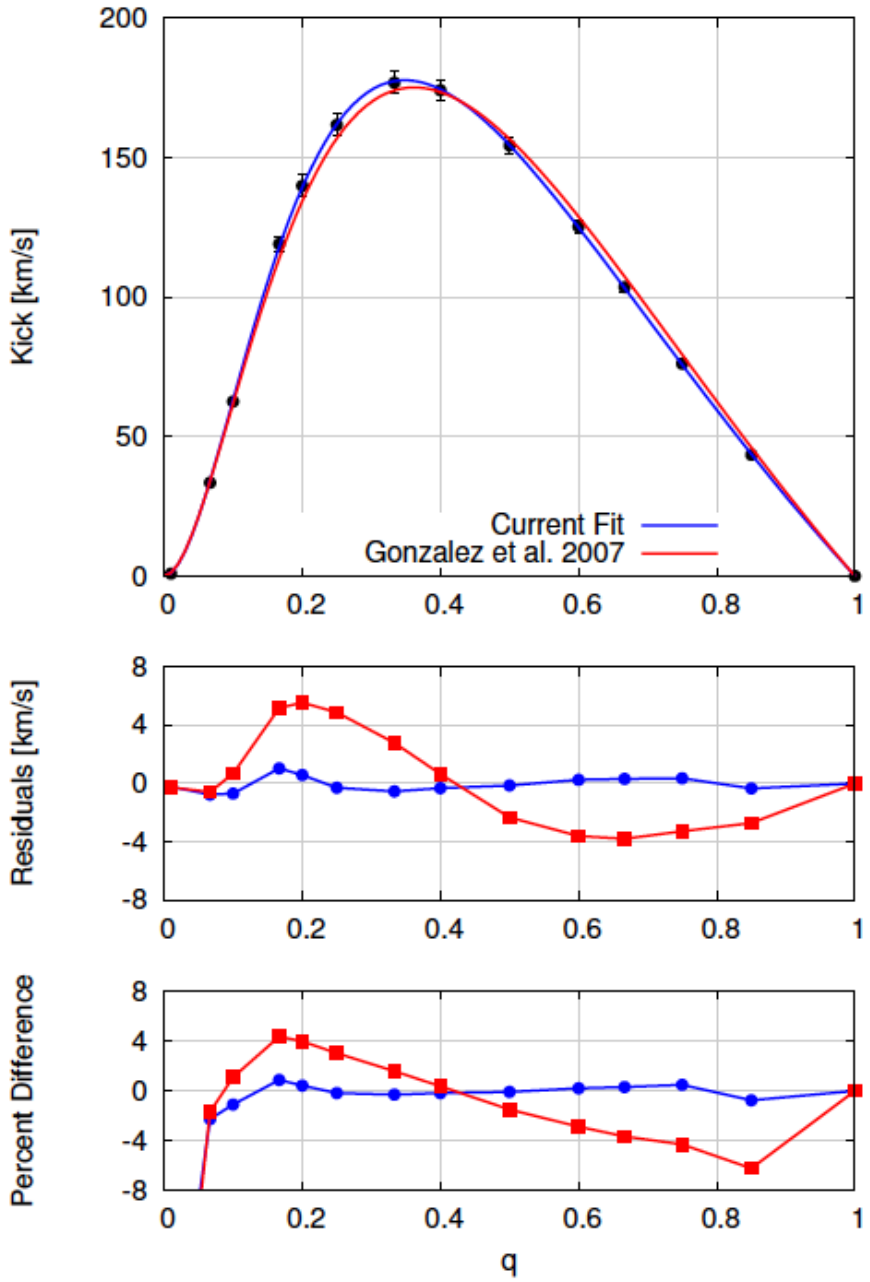

FIG. 1. Our current fit and the original González *et al.* [42] fit to the recoils from nonspinning BHBs. The panel below gives the residual and percent difference of both fits.

B. Peak luminosity of non-Spinning Binaries

$$L_{\rm peak} = (4\eta)^2 \left\{ N_0 + N_{2d}\,\delta m^2 + N_{4f}\,\delta m^4 \right\}. \qquad (2)$$

Note that the radiated power in the particle limit scales as η^2 [see Ref. [43], Eq. (16) and (20); evaluated at the ISCO for its peak value].

[43] R. Fujita, PTEP **2015**, 033E01 (2015), arXiv:1412.5689

TABLE VI. The fitting coefficients for the peak luminosity Eq. (2).

Parameter	L_{peak}
N_0	$1.026 \times 10^{-3} \pm 1.727 \times 10^{-6}$
N_{2d}	$-4.092 \times 10^{-4} \pm 2.847 \times 10^{-5}$
N_{4f}	$2.422 \times 10^{-4} \pm 6.552 \times 10^{-5}$

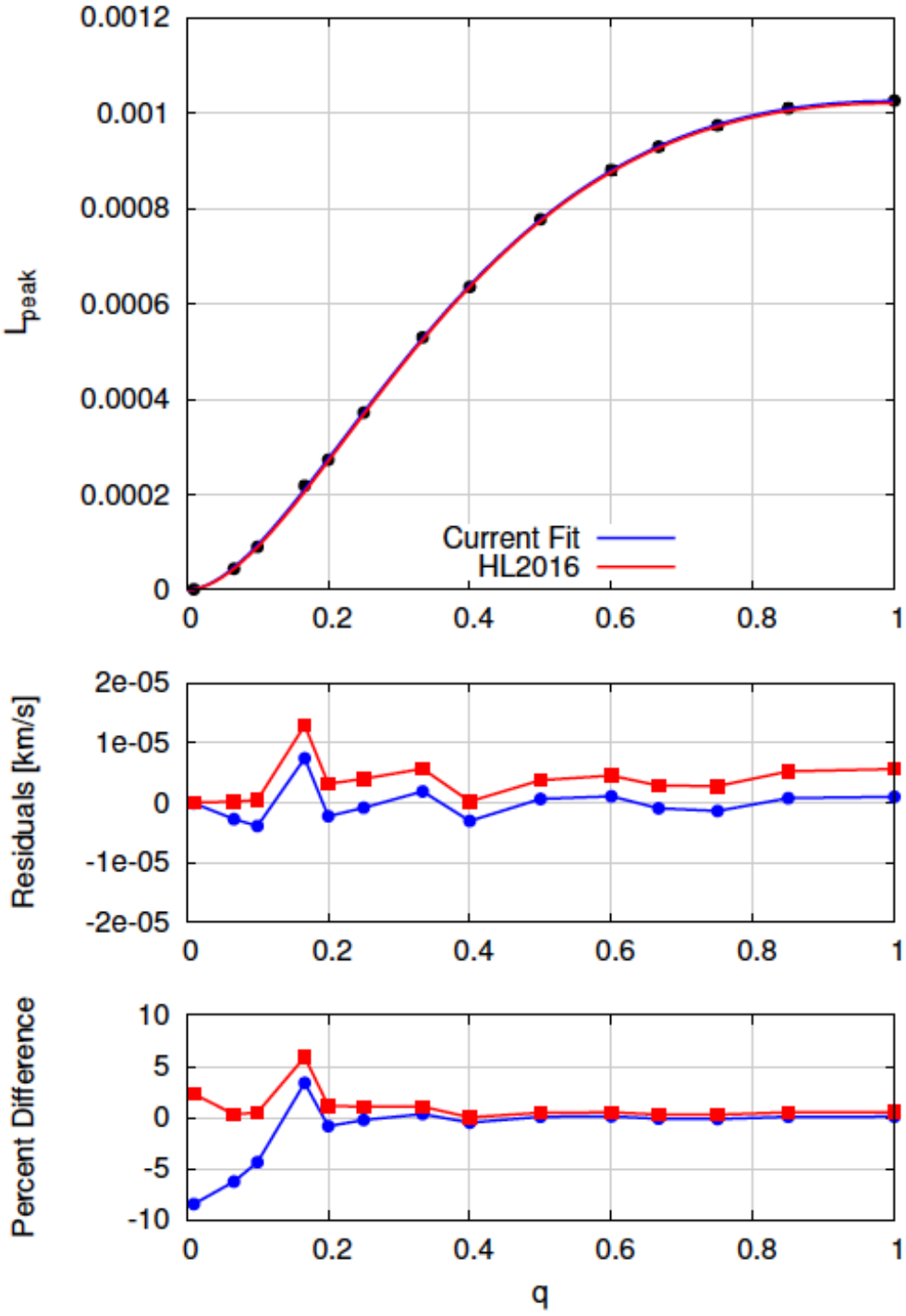

C. Peak frequency and amplitude of non-Spinning Binaries

Analogously to the previous formula to model the peak luminosity, we introduce the following fitting formula for the peak frequency of the $(2,2)$ mode of the gravitational wave strain for nonspinning binaries

$$m\omega_{22}^{\rm peak} = \Big\{ W_0 + W_2\,\delta m^2 + W_4\,\delta m^4 \Big\}, \qquad (3)$$

The results of fitting the parameters W_0, W_2, and W_4

Parameter	Fit 1	Parameter	Fit 2
W_0	0.3587 ± 0.0008	W_0'	0.3580 ± 0.0010
W_2	-0.1211 ± 0.0036	W_2'	0.2466 ± 0.0093
W_4	0.0432 ± 0.0034	W_4'	0.2718 ± 0.0129

If we impose the particle limit peak frequency, $m_f\,\Omega_p = 0.2795$ into our formula, we have the alternative Fit 2:

$$m\omega_{22}^{\rm peak} = (4\eta)\Big\{ W_0' + W_2'\,\delta m^2 + W_4'\,\delta m^4 \Big\} + m_f\,\Omega_p\,\delta m^6, \qquad (4)$$

where $\eta = (1-\delta m^2)/4$.

[44] A. Bohé *et al.*, Phys. Rev. **D95**, 044028 (2017),

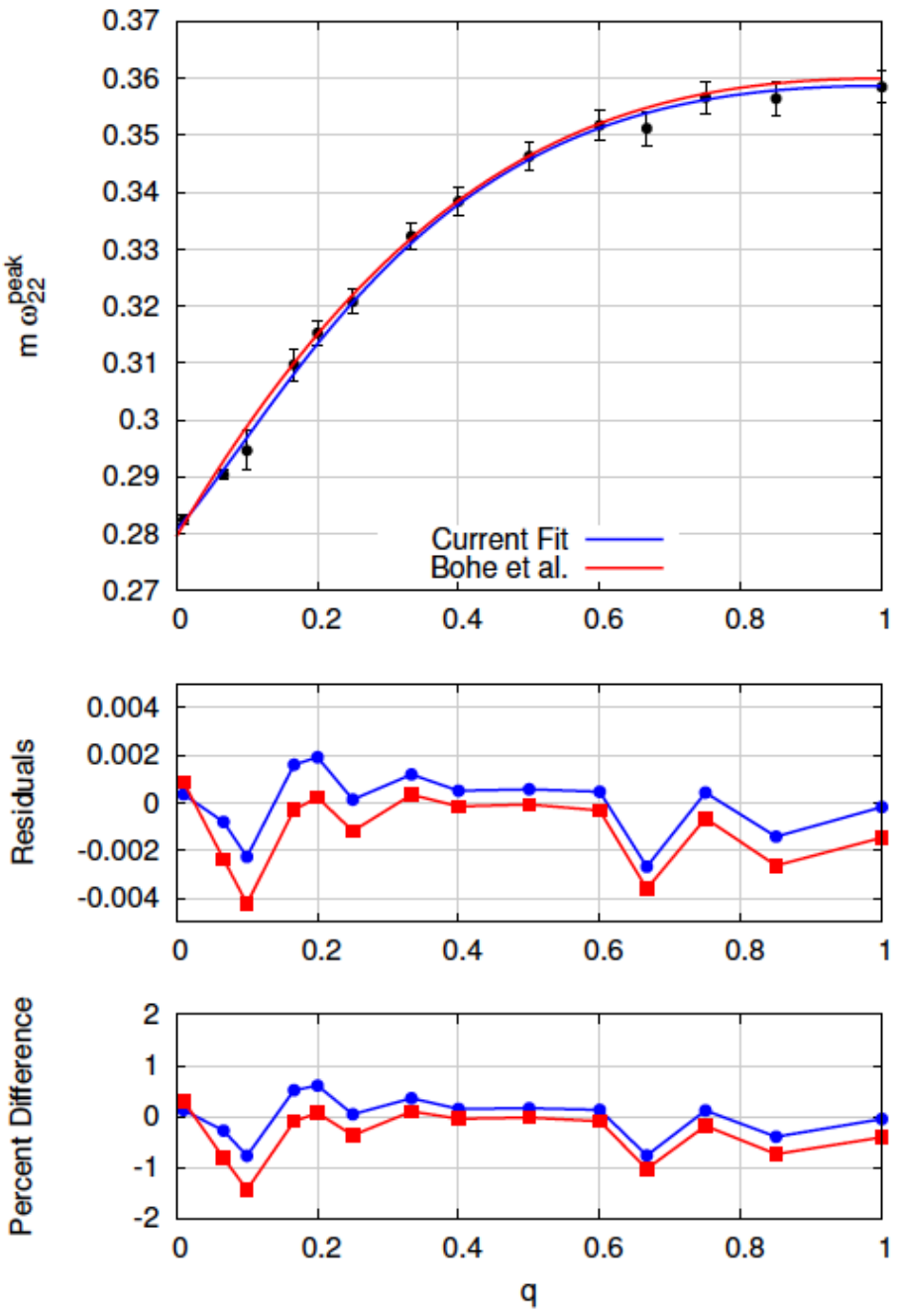

FIG. 3. Current fit and the Bohé *et al.* [44] fit to the peak waveform frequency from nonspinning BHBs.

Final discussion and conclusions

- The particle limit represents a test and a potential improvement for remnant formulae
  - If we have an expression for the particle limit we can readily and effectively incorporate in our formulae with clear benefits, as for m_{final} and Sf_{inal} .
  - NR simulations can also accurately extrapolate from the comparable mass limit and make predictions of what the perturbative, semi-analytic computations should produce.
  - Concrete examples of high accurate computations are the final mass and spin, but the computation of recoil velocities, peak luminosity and peak frequencies would highly benefit of perturbative computations.
  - In particular, the peak frequency can take also an additional η–correction.
  - Should we rerun q=1/100?
  - A predicted h_{peak} - ω_{peak} can be used as a test of GR

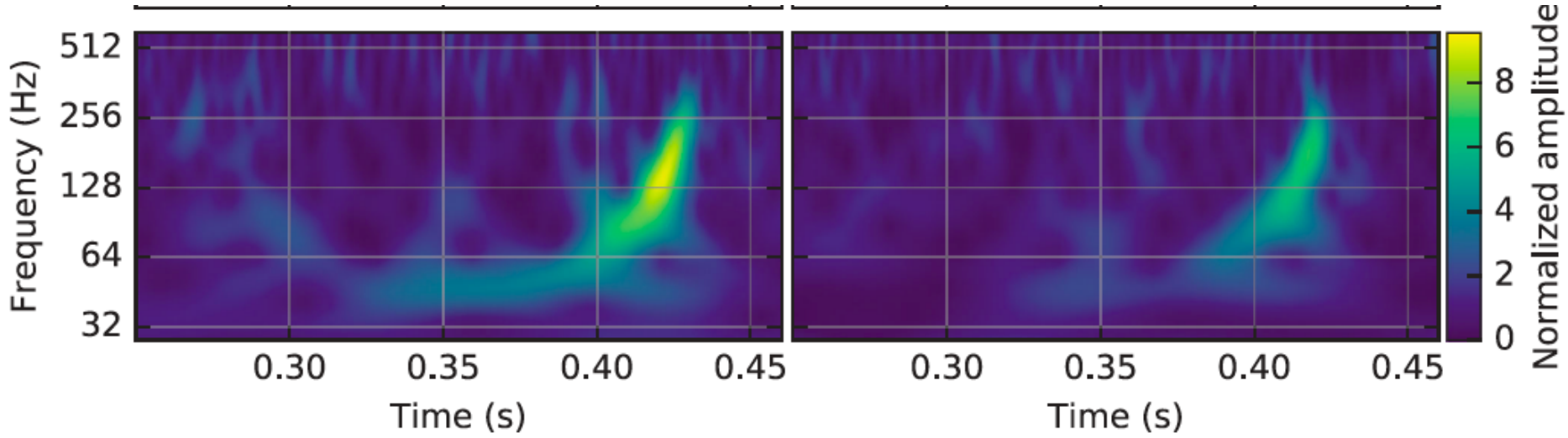

Additional material on the accuracy of the simulations regarding the three main sources of error:
Finite Extraction Radius
Finite Resolution
Finite sum over modes

From appendices in

J. Healy and C. O. Lousto, Phys. Rev. **D95**, 024037 (2017), arXiv:1610.09713 [gr-qc].

J. Healy, C. O. Lousto, and Y. Zlochower, Phys. Rev. **D90**, 104004 (2014), arXiv:1406.7295 [gr-qc].

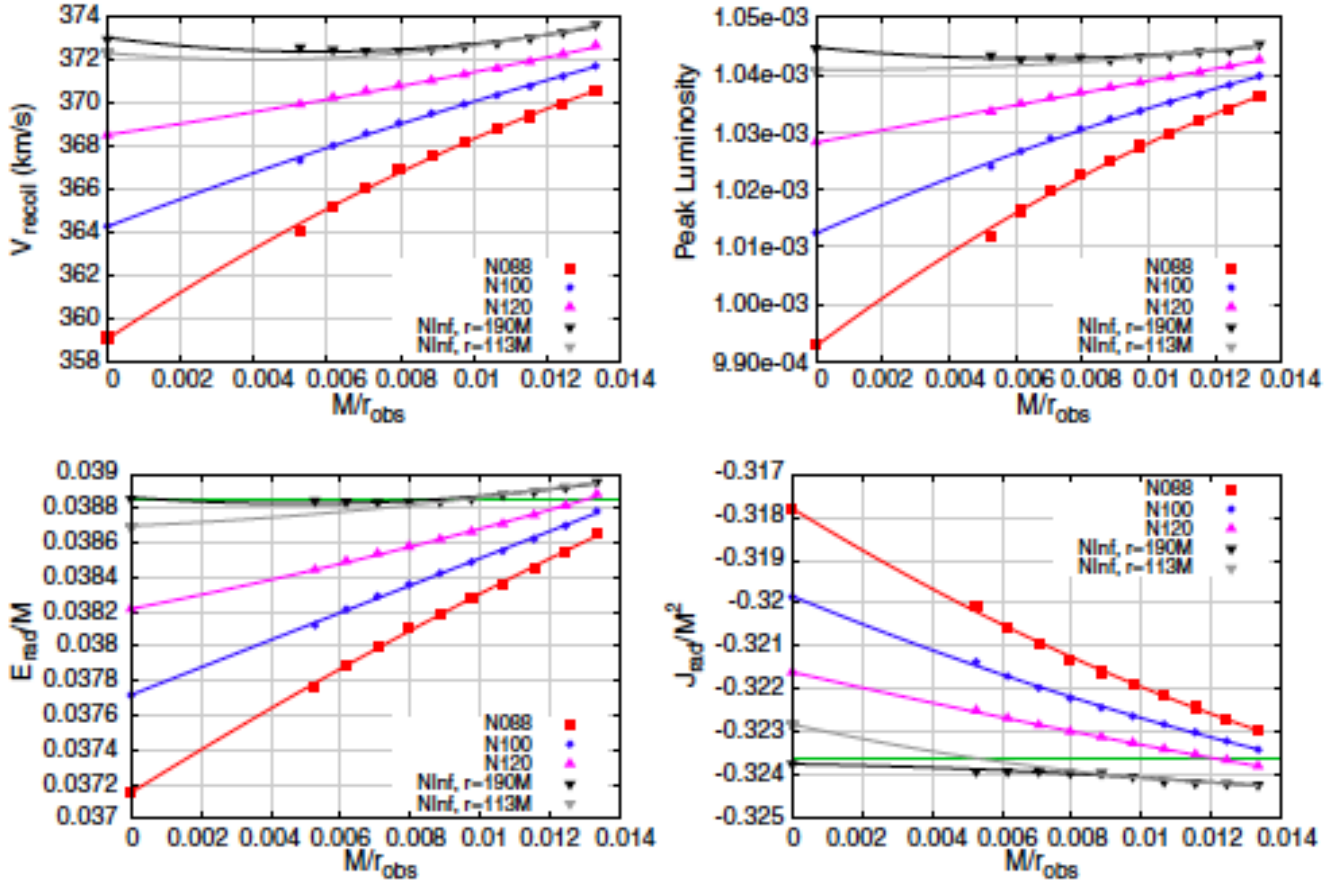

FIG. 8. Plots of the convergence of the recoil velocity (top left), peak luminosity (top right), energy radiated (bottom left), and angular momentum radiated (bottom right) as a function of $m/r_{\rm obs}$ for case 80—Q1.0000_-0.8000_0.8000. Horizontal green solid lines in the bottom row indicate the energy and angular momentum radiated calculated from the isolated horizon. The dark gray lines in each plot shows the extrapolation to infinite observer location using only up to $r = 113$ m.

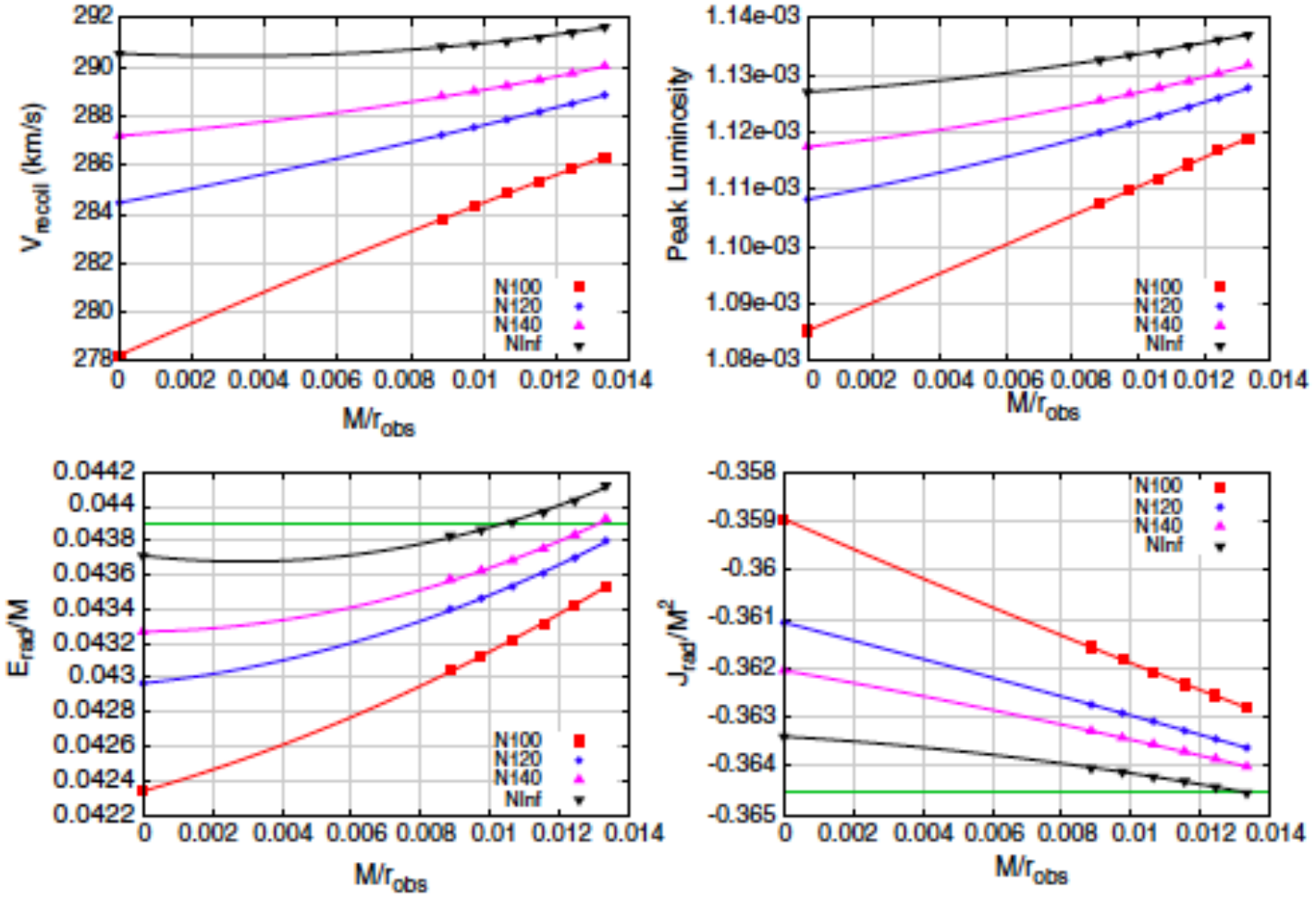

FIG. 9. Plots of the convergence of the recoil velocity (top left), peak luminosity (top right), energy radiated (bottom left), and angular momentum radiated (bottom right) as a function of $m/r_{\rm obs}$ for case 47—Q0.7500_-0.8000_0.8000. Horizontal green solid lines in the bottom row indicate the energy and angular momentum radiated calculated from the isolated horizon.

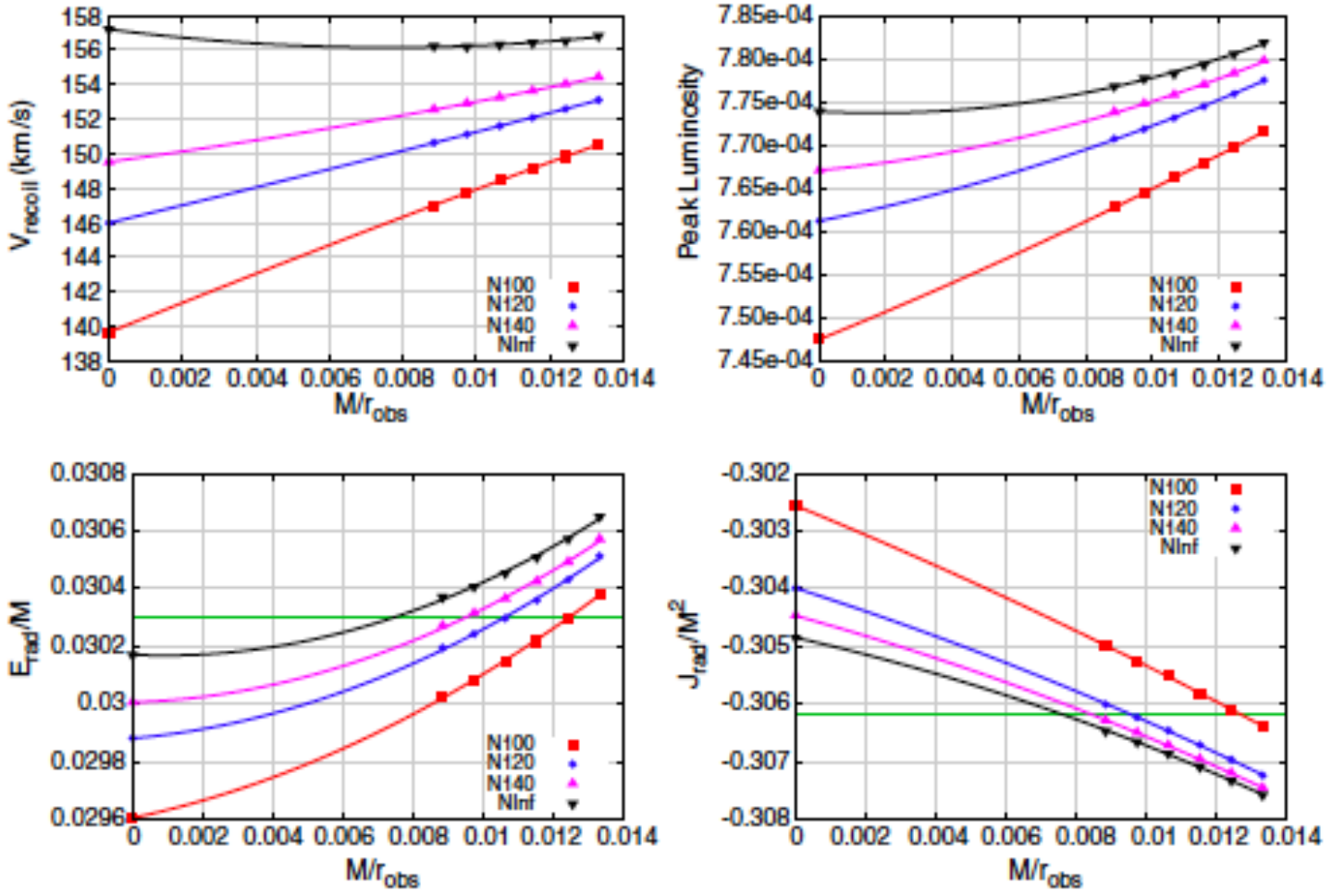

FIG. 10. Plots of the convergence of the recoil velocity (top left), peak luminosity (top right), energy radiated (bottom left), and angular momentum radiated (bottom right) as a function of $m/r_{\rm obs}$ for case 67—Q0.5000_0.0000_0.0000. Horizontal green solid lines in the bottom row indicate the energy and angular momentum radiated calculated from the isolated horizon.

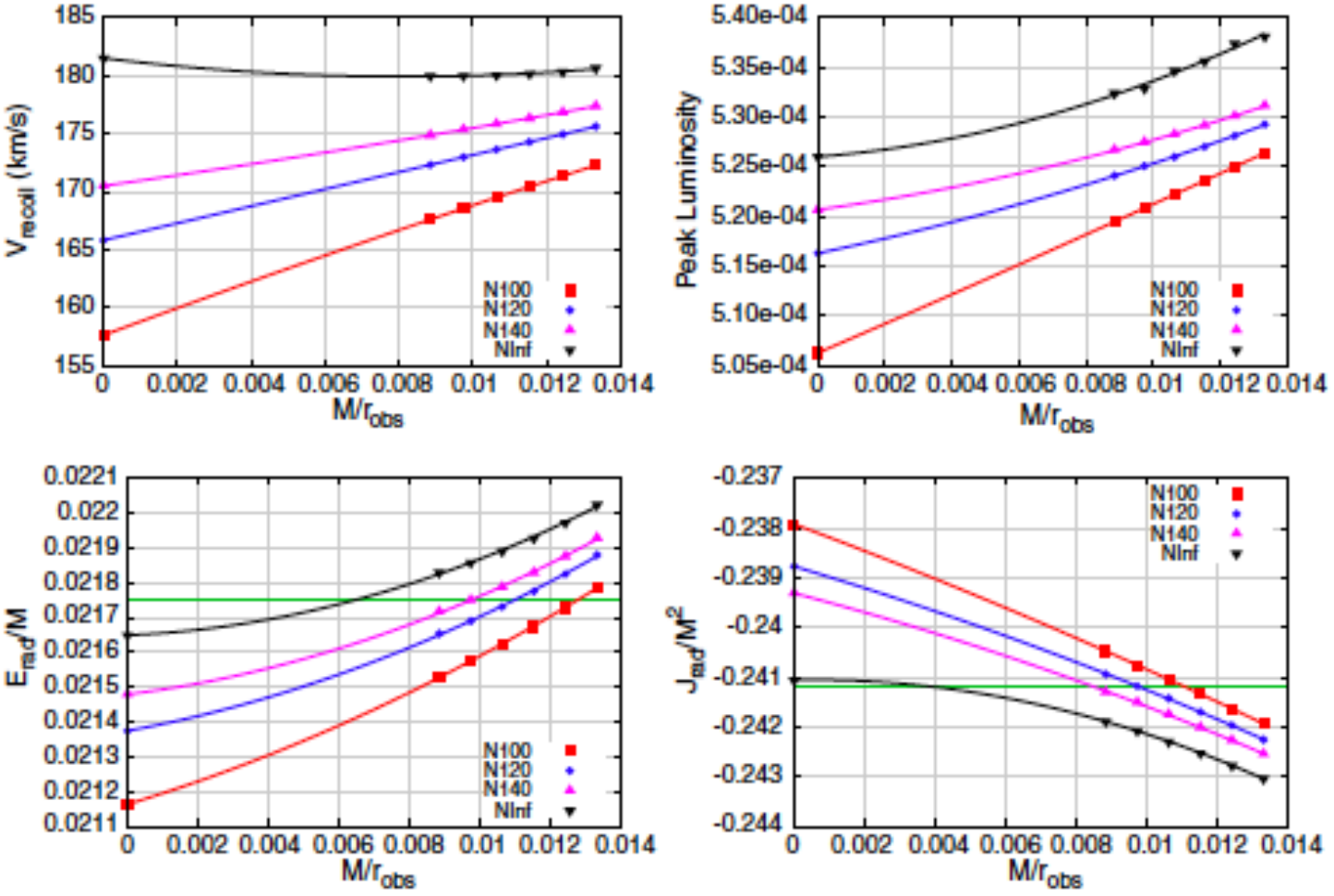

FIG. 11. Plots of the convergence of the recoil velocity (top left), peak luminosity (top right), energy radiated (bottom left), and angular momentum radiated (bottom right) as a function of $m/r_{\rm obs}$ for case 65—Q0.3333_0.0000_0.0000. Horizontal green solid lines in the bottom row indicate the energy and angular momentum radiated calculated from the isolated horizon.

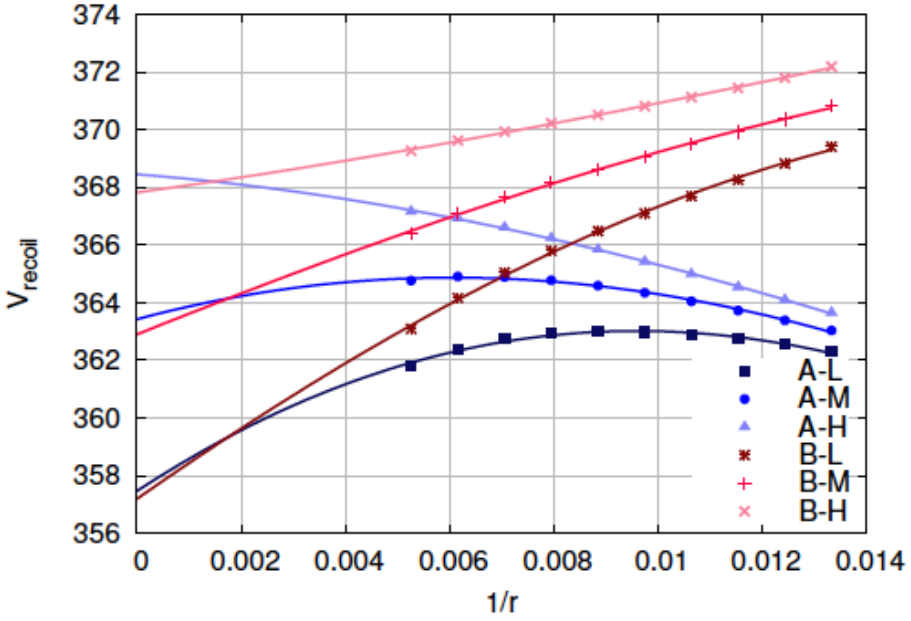

FIG. 22: The recoil velocity as computed at a given extraction radius: $75M - 190M$ and extrapolations to infinity. The different curves correspond to the two initial separations labeled as A and B and as a function of resolution (Low - Medium - High) refined by a global factor 1.2. A quadratic least squares fit is shown for each.

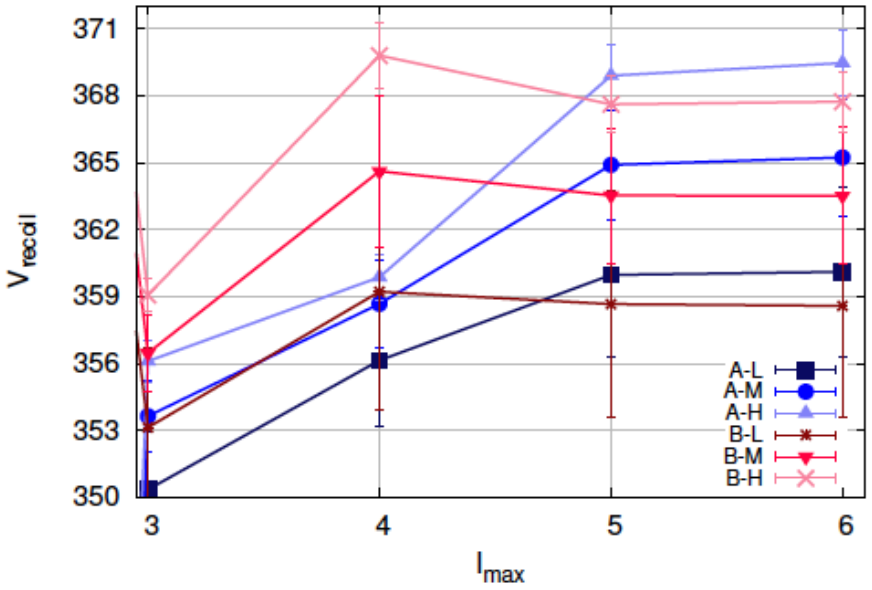

FIG. 23: The dependence of the computed recoil velocity on the number of ℓ modes used to construct the radiated linear momentum. Here all modes with $\ell \leq \ell_{max}$ were used and we show the recoil for the A and B configurations for the Low, Medium, and High resolution runs.

J. Healy, C. O. Lousto, and Y. Zlochower, Phys. Rev. **D90**, 104004 (2014), arXiv:1406.7295 [gr-qc].

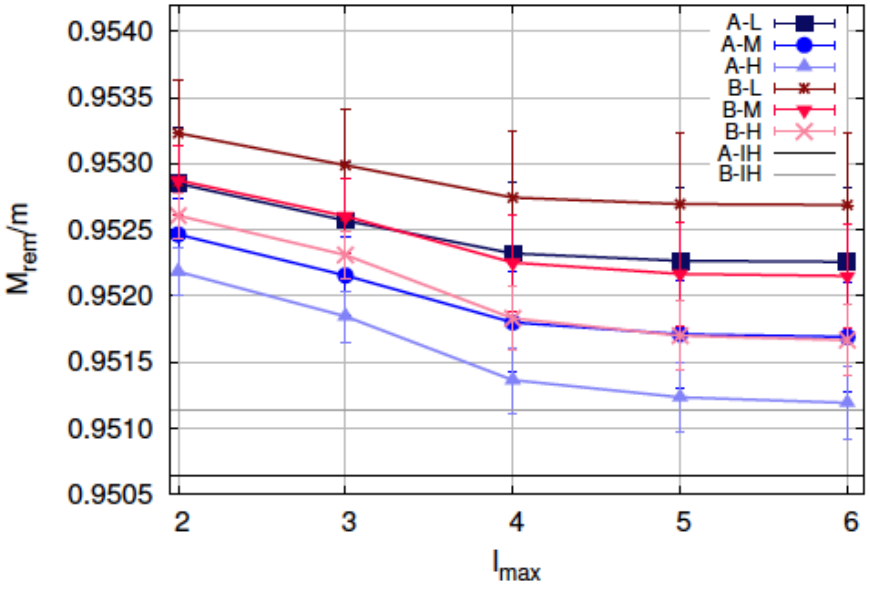

FIG. 24: Above: The radiated energy as computed at a given extraction radius: $75M-190M$ and extrapolations to infinity. The different curves correspond to the two initial separations labeled as A and B and as a function of resolution (Low - Medium - High) refined by a global factor 1.2. A quadratic least squares fit is shown for each. Below: The dependence of the computed radiated energy on the number of ℓ modes used to construct it. Here all modes with $\ell \leq \ell_{\rm max}$ were used. The black and gray lines labeled with "IH" are the associated final mass calculated from the BH horizon. On this scale, all resolutions are on top of one another, so only one line is shown.

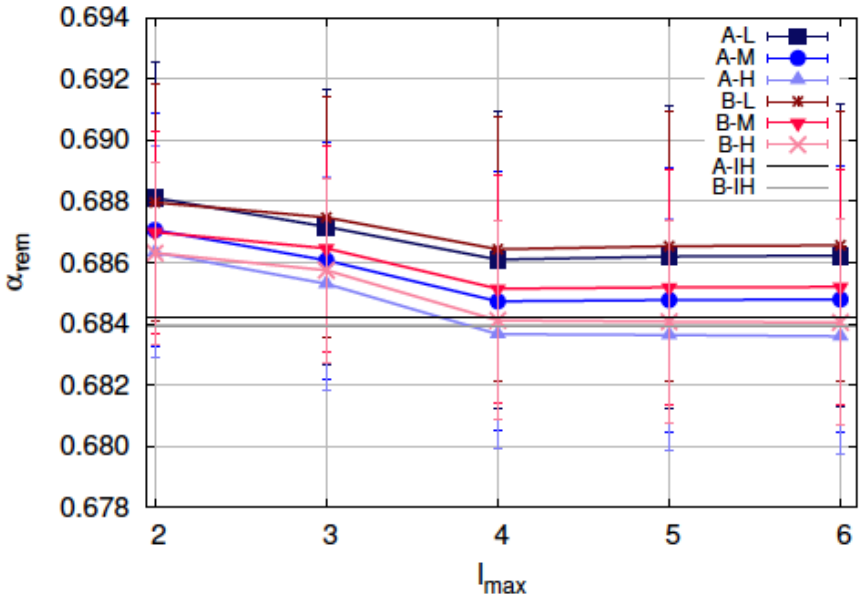

FIG. 25: Above: The radiated angular momentum as computed at a given extraction radius: $75M-190M$ and extrapolations to infinity. The different curves correspond to the two initial separations labeled as A and B and as a function of resolution (Low - Medium - High) refined by a global factor 1.2. A quadratic least squares fit is shown for each. Below: The dependence of the computed radiated angular momentum on the number of ℓ modes used to construct it. Here all modes with $\ell \leq \ell_{\rm max}$ were used. The black and gray lines labeled with "IH" are the associated final spin calculated from the BH horizon. On this scale, all resolutions are on top of one another, so only one line is shown.

J. Healy, C. O. Lousto, and Y. Zlochower, Phys. Rev. **D90**, 104004 (2014), arXiv:1406.7295 [gr-qc].